IVYSPRING INTERNATIONAL PUBLISHER

Theranostics

2017; 7(3): 703-716. doi: 10.7150/thno.16794

Research Paper

Intracellularly Swollen Polypeptide Nanogel Assists Hepatoma Chemotherapy

Bo Shi[1*], Kexin Huang[1*], Jianxun Ding[2*], Weiguo Xu[2✉], Yu Yang[1], Haiyan Liu[1✉], Lesan Yan[3✉], Xuesi Chen[2]

1. Center for Biological Experiment, College of Basic Medicine, Jilin University, Changchun 130021, People's Republic of China;
2. Key Laboratory of Polymer Ecomaterials, Changchun Institute of Applied Chemistry, Chinese Academy of Sciences, Changchun 130022, People's Republic of China.
3. Department of Bioengineering, University of Pennsylvania, Philadelphia, PA 19104-6321, United States of America.

*These authors contributed equally to this work.

✉ Corresponding author: Weiguo Xu, E-mail: wgxu@ciac.ac.cn; Haiyan Liu, E-mail: haiyan@jlu.edu.cn; Lesan Yan, E-mail: lesanyan@gmail.com.

Received: 2016.07.10; Accepted: 2016.12.17; Published: 2017.01.15

Abstract

Nowadays, chemotherapy is one of the principal modes of treatment for tumor patients. However, the traditional formulations of small molecule drugs show short circulation time, low tumor selectivity, and high toxicity to normal tissues. To address these problems, a facilely prepared, and pH and reduction dual-responsive polypeptide nanogel was prepared for selectively intracellular delivery of chemotherapy drug. As a model drug, doxorubicin (DOX) was loaded into the nanogel through a sequential dispersion and dialysis technique, resulting in a high drug loading efficiency (DLE) of 96.7 wt.%. The loading nanogel, defined as NG/DOX, exhibited a uniform spherical morphology with a mean hydrodynamic radius of 58.8 nm, pH and reduction dual-triggered DOX release, efficient cell uptake, and cell proliferation inhibition *in vitro*. Moreover, NG/DOX exhibited improved antitumor efficacy toward H22 hepatoma-bearing BALB/c mouse model compared with free DOX·HCl. Histopathological and immunohistochemical analyses were implemented to further confirm the tumor suppression activity of NG/DOX. Furthermore, the variations of body weight, histopathological morphology, bone marrow cell micronucleus rate, and white blood cell count verified that NG/DOX showed excellent safety *in vivo*. With these excellent properties *in vitro* and *in vivo*, the pH and reduction dual-responsive polypeptide nanogel exhibits great potential for on-demand intracellular delivery of antitumor drug, and holds good prospect for future clinical application.

Key words: Polypeptide Nanogel, Stimuli-Responsiveness, Intracellular Drug Delivery, Hepatoma Chemotherapy.

Introduction

Chemotherapy is a conventional treatment approach for cancer patients, which has played a key role in clinical application for many decades [1, 2]. Although a variety of new antitumor drugs are developed constantly, chemotherapy is still limited by many disadvantageous factors, such as rapid drug metabolism and severe side effects [3, 4]. The recent development of nanotechnologies for drug delivery provides a vigorous measure to cover the shortcomings of antitumor drugs [5, 6]. Currently, different polymer nanoparticles, *e.g.*, micelles [7, 8], vesicles [9, 10], and nanogels [11, 12], have been prepared and used to controllably deliver many clinically important antineoplastic agents [13]. These smart drug delivery systems can prolong circulation time in the blood and enhance intratumoral accumulation through the enhanced permeability and retention (EPR) effect, thus increasing the therapeutic effect and diminishing adverse reactions [14].

Compared with normal tissues, solid tumors exhibit characteristic microenvironments, such as hypoxia, high lactate level, and extracellular acidosis

[15]. Most interestingly, tumors have an acidic and reductive intracellular microenvironment [16]. Significant differences in pH and concentration of glutathione (GSH) exist between intracellular and extracellular spaces [17, 18]. Endosomal pH is approximately 5.0 − 6.5; intracellular GSH concentration is 50 to 1000 times higher than extracellular one [8, 19]. Based on these properties, various kinds of stimuli-responsive polymer nanoparticles have been exploited for antitumor drug delivery [11, 20]. Among them, nanogels, as a type of cross-linked polymer nanoparticle, demonstrate a good prospect for drug delivery. The excellent capability of controlled drug release benefits from tunable and stable chemical and three-dimensional (3D) physical structures, stimuli-responsiveness, and high drug loading capability [21, 22]. After the nanogels are administrated into body by intravenous injection, the drug-loaded nanogels are selectively accumulated within the tumor site through the EPR effect. Once the nanogels are uptaken by tumor cells, the intracellular microenvironment triggers the immediate release of payloads [20, 23].

In the past five years, our group has synthesized and characterized a series of microenvironment-responsive nanogels for smart antitumor drug delivery [7, 8, 24-27]. Notably, the reduction-responsive polypeptide nanogels were synthesized by the ring-opening polymerization (ROP) of monofunctional and difunctional amino acid *N*-carboxyanhydrides (NCAs) [25, 28]. Based on the previous studies, the pH and reduction dual-responsive nanogel of methoxy poly(ethylene glycol)−poly(L-glutamic acid-*co*-L-cystine) (mPEG−P(LG-*co*-LC)) was synthesized by the one-step ROP of γ-benzyl-L-glutamate *N*-carboxyanhydride (BLG NCA) and L-cystine *N*-carboxyanhydride (LC NCA), and subsequent deprotection of γ-benzyl group. Specifically, a model antitumor drug doxorubicin (DOX) was loaded into nanogel for the selectively intracellular delivery of antitumor drug *in vitro* and *in vivo* in this study (Scheme 1). The resulting nanoparticle, referred to as NG/DOX, showed pH and reduction dual-dependent release behavior and efficient capability for inhibiting cell proliferation *in vitro*. Even more importantly, NG/DOX demonstrated enhanced tumor growth suppression and improved safety *in vivo* compared with free doxorubicin hydrochloride (DOX·HCl). Altogether, NG/DOX exhibited great potential for the clinical chemotherapy of malignancy.

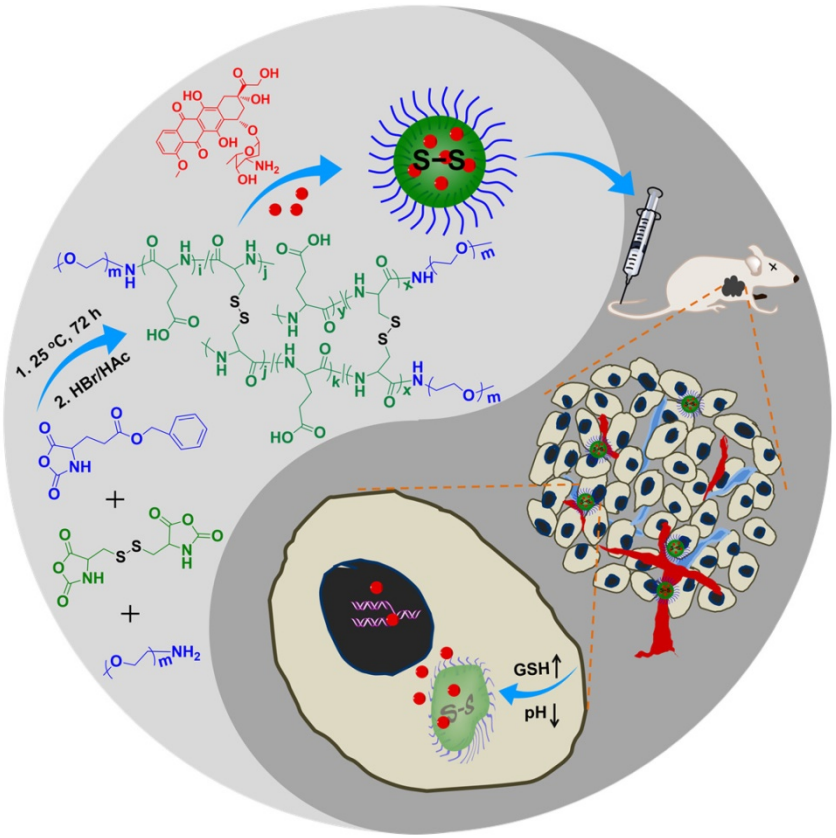

Scheme 1. Synthetic pathway for mPEG−P(LG-*co*-LC) nanogel, illustration of DOX encapsulation by nanogel, and its circulation, intratumoral accumulation, endocytosis, and targeted intracellular DOX release after intravenous injection.

Materials and Methods

Materials

$mPEG_{113}$−P(LG_{35}-*co*-LC_8) was synthesized according to our previously reported protocol [25]. The subscript number represented the degree of polymerization (DP) of each moiety, which was calculated from elemental analysis. DOX·HCl was purchased from Beijing Huafeng United Technology Co., Ltd. (Beijing, P. R. China). GSH (used for cell culture) and sodium dodecyl sulfonate (SDS) were purchased from Aladdin Reagent Co., Ltd. (Shanghai, P. R. China). Cell culture products including Dulbecco's modified Eagle's medium (DMEM), Roswell Park Memorial Institute (RPMI) 1640 medium, and fetal bovine serum (FBS) were provided by Gibco (USA). Penicillin and streptomycin were obtained from Huabei Pharmaceutical Co., Ltd. (Shijiazhuang, P. R. China). 3-(4,5-Dimethyl-thiazol-2-yl)-2,5-diphenyl tetrazolium bromide (MTT) was purchased from Sigma-Aldrich (Shanghai, P. R. China). 4′,6-Diamidino-2-phenylindole dihydrochloride (DAPI) was purchased from Thermo Fisher Scientific (Lafayette, Colorado, USA). Hematoxylin and eosin were obtained from Merck Company (Darmstadt, Germany). The purified deionized water was prepared by the Milli-Q plus system (Millipore Co., Billerica, MA, USA). The antibodies of p53, Fas, tumor necrosis factor-α (TNF-α), and cyclin E were purchased from Abcam Company (Cambridge, UK). SP9710 and diaminobenzidine (DAB) chromogenic kits were purchased from Fuzhou Maixin Biotechnology Development Company (Fuzhou, P. R. China).

DOX encapsulation

As shown in Scheme 1, DOX was loaded into the core of nanogel through a sequential dispersion and dialysis approach. Briefly, nanogel (50.0 mg) was first dispersed in 20.0 mL of *N,N*-dimethylformamide (DMF), and then DOX·HCl (10.0 mg) was dissolved in the above solution and further stirred for 12 h at room temperature. Subsequently, 2.0 mL of phosphate-buffered saline (PBS; 0.01 M, pH 7.4) and 18.0 mL of MilliQ water were rapidly added into the above mixture. The resulting solution was stirred for 12 h at room temperature and subsequently dialyzed against MilliQ water for 24 h (molecular weight cut-off (MWCO) = 3500 Da). The MilliQ water was replaced every 2 h. Finally, NG/DOX was obtained by lyophilization after filtration.

To detect the drug loading content (DLC) and drug loading efficiency (DLE), 1.0 mg of drug-loaded nanogel was dissolved in 10.0 mL of DMF and stirred for 12 h at room temperature. The quantity of drug in nanogel was detected through fluorescence spectroscopy on a Photon Technology International (PTI) Fluorescence Master System with Felix 4.1.0 software (PTI, Lawrenceville, NJ, USA; λ_{ex} = 480 nm). The DLC and DLE of NG/DOX were calculated by Equations (1) and (2), respectively.

$$\text{DLC (wt.\%)} = \frac{\text{Weight of Drug in Nanogel}}{\text{Weight of Drug-Loaded Nanogel}} \times 100\% \quad (1)$$

$$\text{DLE (wt.\%)} = \frac{\text{Weight of Drug in Nanogel}}{\text{Total Weight of Feeding Drug}} \times 100\% \quad (2)$$

Characterizations

Transmission electron microscopy (TEM) measurements were performed on a JEOL JEM-1011 transmission electron microscope with an accelerating voltage of 100 kV. To prepare the TEM sample, NG or NG/DOX was dissolved in PBS at a concentration of 50.0 μg mL^{-1}, and then dropped on a carbon-coated copper grid and dried at room temperature for over one day in the air. Dynamic light scattering (DLS) measurements were performed with a vertically polarized He−Ne laser (DAWN EOS, Wyatt Technology). To prepare the DLS sample, NG or NG/DOX was dissolved in PBS at a concentration of 100.0 μg mL^{-1}.

DOX release

To determine the release profiles of DOX, the weighed freeze-dried NG/DOX was suspended in 10.0 mL of PBS at different pH values of 4.9, 6.8, and 7.4 without or with 10.0 mM GSH, and then transferred into a dialysis bag (MWCO = 3500 Da). The release experiment was initiated by placing the end-sealed dialysis bag into 100.0 mL of corresponding release medium at 37 °C with constant shaking at 75 rpm. At preselected time intervals, 2.0 mL of release medium was taken out and replenished with an equal volume of fresh medium. The amount of released DOX was determined using fluorescence spectroscopy (λ_{ex} = 480 nm, λ_{em} = 590 nm).

Cell culture

Human hepatoma HepG2 cells were cultured in DMEM, while mouse hepatoma H22 cells were cultured in RPMI 1640 medium, both supplemented with 10% (*V*/*V*) fetal bovine serum (FBS), penicillin (50.0 IU mL^{-1}), and streptomycin (50.0 IU mL^{-1}) at 37 °C in 5% (*V*/*V*) carbon dioxide (CO_2).

Intracellular DOX release

The cell uptake and intracellular DOX release from NG/DOX toward HepG2 and H22 cells were detected by both confocal laser scanning microscopy (CLSM) and flow cytometry (FCM).

The cells were seeded in 6-well plates on the coverslips with a density of 1.5×10^5 cells per well in 2.0 mL of culture medium. Cells were cultured for 12 h and then pretreated without or with 10.0 mM GSH for 2 h. Then the culture medium was removed, and the cells were washed three times with PBS. Next, each well was treated with 1.0 mL of NG/DOX solution in culture medium at pH 7.4 with a final DOX·HCl dose of 10.0 μg mL^{-1}. Alternatively, as a control, cells were given an equivalent dose of free DOX·HCl without GSH pretreatment. After incubation for another 2 h, the cells were washed three times with PBS and fixed with 4% (*W*/*V*) PBS-buffered paraformaldehyde for 30 min at room temperature. Subsequently, the cell nuclei were stained with DAPI for 3 min at room temperature. The intracellular localization of DOX was visualized under a CLSM (Carl Zeiss, LSM 780, Jena, Germany).

In a similar technique, cells were seeded in 6-well plates, pretreated without or with 10.0 mM GSH for 2 h, and co-incubated with NG/DOX solution in culture medium at pH 7.4 and a final DOX·HCl dose of 10.0 μg mL^{-1} for another 2 h. Control cells were given the equivalent dose of free DOX·HCl without GSH pretreatment. Subsequently, the cells were washed three times with PBS and digested with 0.25% (*W*/*V*) trypsin/EDTA. EDTA is the abbreviation of ethylenediaminetetraacetate (EDTA). The harvested cells were suspended in PBS and centrifuged at 1500 rpm and 4 °C for 5 min. The supernatants were discarded, and the cells were washed with PBS to remove background fluorescence in the medium. After two cycles of washing and centrifugation, the cells were resuspended with 400.0 μL of PBS. FCM detection was performed using a BD FACSCalibur flow cytometer (BD Biosciences, San Jose, CA, USA).

Cytotoxicity assays

The cytotoxicities of free DOX·HCl and NG/DOX were evaluated by MTT assay. Briefly, 1×10^4 cells per well were seeded in 96-well plates in 150.0 μL of culture medium at pH 7.4, incubated for 12 h, and then pretreated with 10.0 mM GSH for 2 h. Cells without GSH pretreatment were used as a control. The culture medium was removed, and the cells were washed three times with PBS. Subsequently, each well was given 200.0 μL of fresh media at pH 7.4 containing free DOX·HCl or NG/DOX at different DOX·HCl doses from 10.0 to 0.156 μg mL^{-1}. After 48 h incubation, 20.0 μL of MTT solution was added, and cells were incubated for another 4 h. Then, 100.0 μL of SDS-isobutanol-HCl (10% (*W*/*V*) SDS, 5% (*V*/*V*) isobutanol, and 10.0 μM HCl) were added to each well and incubated for 12 h at 37 °C. The absorbance of the above solution at 570 nm was measured on an ELx808 microplate reader (Bio-Tek Instruments, Inc., Winooski, VT, USA). The relative cell viability was calculated by comparing the absorbance with a control well containing no DOX formulations (Equation 3).

$$\text{Cell Viability (\%)} = \frac{A_{\text{sample}}}{A_{\text{control}}} \times 100\% \quad (3)$$

In Equation (3), the control group was maintained without any treatment.

Animal procedures

Six-week-old female Wistar rat weighing 190 ± 20 g and 5-week-old male BALB/c mice weighing 20 ± 0.3 g were provided by the Animal Center of Jinlin University (Changchun, P. R. China). All animal experiments were conducted in accordance with the Guidelines for Animal Care and Use Committee of Jilin University, and all efforts were made to minimize suffering. The hepatoma-grafted mouse model was constructed by subcutaneous injection in the armpit of right forelimb with 100.0 μL of cell suspension containing 2.0×10^6 H22 cells in PBS.

Pharmacokinetic detections

The rats were stabilized under normal conditions for three days and then randomly divided into two groups (n = 5). DOX and NG/DOX were administered intravenously *via* tail vein at an equivalent DOX·HCl dose of 15.0 mg per kg body weight (mg (kg BW)$^{-1}$). The blood samples were collected after 10 and 30 min, and 1, 3, 6, 12, and 24 h after injection. The content of DOX in the blood samples was determined by high-performance liquid chromatography (HPLC; Waters e2695 Separations Module, Waters Co., Milford, MA, USA). Briefly, a 150.0 μL of plasma sample was deproteinized with 1.0 mL of methanol and 20.0 μL of daunorubicin hydrochloride (DAU·HCl) at a concentration of 10.0 μg mL^{-1} as an internal standard. Subsequently, the mixture was vortexed for 10 min and centrifuged at 10,000 rpm for 5 min. Then 600.0 μL of supernatant was collected and dried under a stream of nitrogen (N_2) at 35 °C. The dried sample was dissolved in the mobile phase for HPLC analysis. For HPLC analysis, C-18 column (250 mm × 4.6 mm; WondaCract ODS-2) was used. The mobile phase consisted of a mixture of water:methanol (3:7, *V*/*V*) containing 20.0 mM monopotassium. Detection was carried out using a fluorescence detector (Waters 2475 Multi λ Fluorescence Detector, Waters Co., Milford, MA, USA; λ_{ex} = 480 nm, λ_{em} = 590 nm). The flow was 1.0 mL min^{-1}. All the data was calculated with PKSolver program (Version 2.0; China Pharmaceutical University, Nanjing, P. R. China).

In vivo antitumor assessments

Beginning in the fourth day after the inoculation of H22 hepatoma, that is, day 1, the tumor size and body weight were monitored every two days. After five days, the tumor mass grew to approximately 140.0 mg, and then the mice were randomly divided into five groups (n = 10), *i.e.*, normal saline (NS), or DOX·HCl or NG/DOX at a DOX·HCl dose of 3.0 or 6.0 mg (kg BW)$^{-1}$. The DOX formulations were noted as DOX/3.0, DOX/6.0, NG/DOX/3.0, and NG/DOX/6.0, respectively. Treatments were begun concomitantly, and consisted of 200.0 μL of NS and various DOX formulations in NS, injected into the tail vein once every five days for a total of four injections in 25 days. The antitumor efficacies of various formulations *in vivo* were evaluated by detecting the tumor weight (Equation 4) [29] and tumor index (Equation 5). Body weight was real-time monitored for safety assessment.

$$\text{Tumor Weight (mg)} = \frac{L \times S^2}{2} \times (1.0\ \text{mg mm}^{-3}) \quad (4)$$

$$\text{Tumor Index (mg g}^{-1}) = \frac{\text{Tumor Weight (mg)}}{\text{Body Weight (g)}} \quad (5)$$

In Equation (4), L and S (mm) were the largest (L) and smallest (S) diameters of tumor, respectively.

Histopathological and immunohistochemical analyses of tumor tissues

The H22 hepatoma-grafted BALB/c mice were sacrificed by cervical dislocation on day 25, *i.e.*, five days after the final injections. The tumors were isolated and fixed in 4% (W/V) paraformaldehyde for 24 h, followed by dehydration, clearing, wax infiltration, and embedding. Approximately 5 μm thick paraffin sections were prepared for hematoxylin and eosin (H&E) staining, and paraffin sections of ~ 3 μm thick were prepared for immunohistochemical staining, including p53, Fas, TNF-α, and cyclin E, in order to assess the pathological and immunological changes in tumor tissues, respectively. The instruments used were Leica RM 2245 paraffin machine (Leica, Germany), Leica HI1210 fishing machine (Leica, Germany), Leica HI1220 booth machine (Leica, Germany), Leica EG1150H embedding machine (Leica, Germany), Olympus BX51 microscope (Olympus, Japan), and Motic image analysis system (Motic Industrial Group Co., Ltd.; Xiamen, P. R. China).

Histopathological assays of sternums and detections of bone marrow cell micronucleus rates (BMMRs)

In addition, sections of sternum from BALB/c mice were placed in 10% (V/V) formic acid-formalin solution, decalcified, and fixed for 10 days. Data from non-grafted mice were used as a control. Next, the tissues were dehydrated, followed by clearing, wax infiltration, and embedding. Four paraffin sections with a thickness of ~ 5 μm for each sternum were collected with an interval of 50.0 μm for H&E staining. The BMMR was evaluated from the H&E-stained section.

White blood cell (WBC) count determinations

On day 25, 20.0 μL of anticoagulated blood from each mouse were obtained *via* retro-orbital to count the quantity of WBCs.

Statistical analyses

All tests were implemented at least three times, and the data were expressed as mean ± standard deviation (SD). Statistical analyses were performed using SPSS 13.0 for Windows (SPSS Inc., Chicago, IL, USA). $P < 0.05$ was considered statistically significant, and $P < 0.01$ and $P < 0.001$ were considered highly significant.

Results and Discussion

DOX encapsulation and NG/DOX characterizations

As shown in Scheme 1, the pH and reduction dual-responsive mPEG−*b*-P(LG-*co*-LC) nanogel was synthesized through the one-step ROP of LG NCA and LC NCA with amino-terminated mPEG (mPEG-NH_2) as a macroinitiator. The prepared smart nanogel was comprised of a hydrophilic mPEG shell and a hydrophobic disulfide-cross-linked P(LG-*co*-LC) core. The mPEG component gave the nanogel a "stealth" feature and permitted an extended half-life within the blood circulation. The LG moiety improved the drug loading capability of nanogel through the electrostatic interaction between the carboxyl group in LG and amino group in drug, and gave the nanogel pH-sensitivity upon protonation or deprotonation. The segment of LC consisting of disulfide bond (S−S) endowed the nanogel with reduction-responsiveness. DOX, a model hydrophobic antitumor drug, was loaded into the core of nanogel through dispersion (Scheme 1). The DLC and DLE of NG/DOX were calculated to be 16.1 and 96.7 wt.%, respectively. The nanogel morphology and size were further studied by TEM and DLS, as depicted in Figure 1. Both NG and NG/DOX exhibited a regular spherical morphology, as measured by TEM. The mean radius of NG measured by TEM was 42.5 nm (Figure 1A). After drug loading, it changed to 55 nm (Figure 1B). DLS studies showed that the hydrodynamic radii (R_hs) of NG and NG/DOX were 53.5 ± 3.4 and 58.8 ± 2.9 nm,

respectively (Figure 1). The particle sizes measured by TEM agreed well with that measured by DLS. Previous studies have reported that nanoparticles with diameter around 100 nm showed long blood circulation and a high propensity of extravasation through tumor vascular fenestrations [30]. Therefore, the size of NG/DOX is conducive to the selective aggregation in the tumor site through the EPR effect.

Prior to evaluating whether NG/DOX is a suitable antitumor agent for *in vitro* and *in vivo* studies, the stability of NG and NG/DOX in different conditions was shown. As can be seen from Figure 1C and 1D, no remarkable size changes were observed over 96 h in PBS at different pH values (*i.e.*, 4.9, 6.8, and 7.4), indicating that the blank and loading nanogel were stable at physiological pH. However, when GSH was added, an obvious swelling and even disassembly of NG or NG/DOX was observed over the time course of the test duration, indicating that the nanogels were instable in the redox intracellular conditions, resulting in the accelerated drug release and, therefore improved the antitumor efficacy.

In vitro DOX release and cell proliferation inhibition

The release profiles of DOX from NG/DOX were determined in PBS with 0 or 10.0 mM GSH at varied pH values (*i.e.*, 4.9, 6.8, and 7.4) and 37 °C with constant shaking of 75 rpm mimicking heart rate, and the results were plotted in Figure 2. No initial burst release was observed; instead, a reduction-dependent DOX release behavior was revealed. At pH 7.4 and without GSH, less than 33.0% of loaded DOX was released from nanogel into the medium over the entire course of the test duration (*i.e.*, 72 h). As expected, lower pH and higher GSH concentration significantly accelerated the release of DOX from the pH and reduction dual-responsive NG/DOX. In the initial 24 h, the percentages of cumulative DOX release in PBS without GSH were 47.5% at pH 4.9, 35.7% at pH 6.8, and 23.4% at pH 7.4. The pH-dependent release behavior likely resulted from a decrease in the electrostatic interaction between nanogel and DOX upon protonation of the carboxyl group in the core of nanogel. However, in the presence of 10.0 mM GSH, the values became 74.6%, 68.6%, and 56.5%, respectively. After incubation for 72 h, more than 88.3% of loaded DOX released from NG/DOX in the medium with GSH at pH 4.9. Given the appreciable difference in redox potential and pH value between extracellular and intracellular microenvironments, NG/DOX is likely to display distinct release behavior in these two locations with greater drug delivery within tumor cells, resulting in a higher antitumor activity.

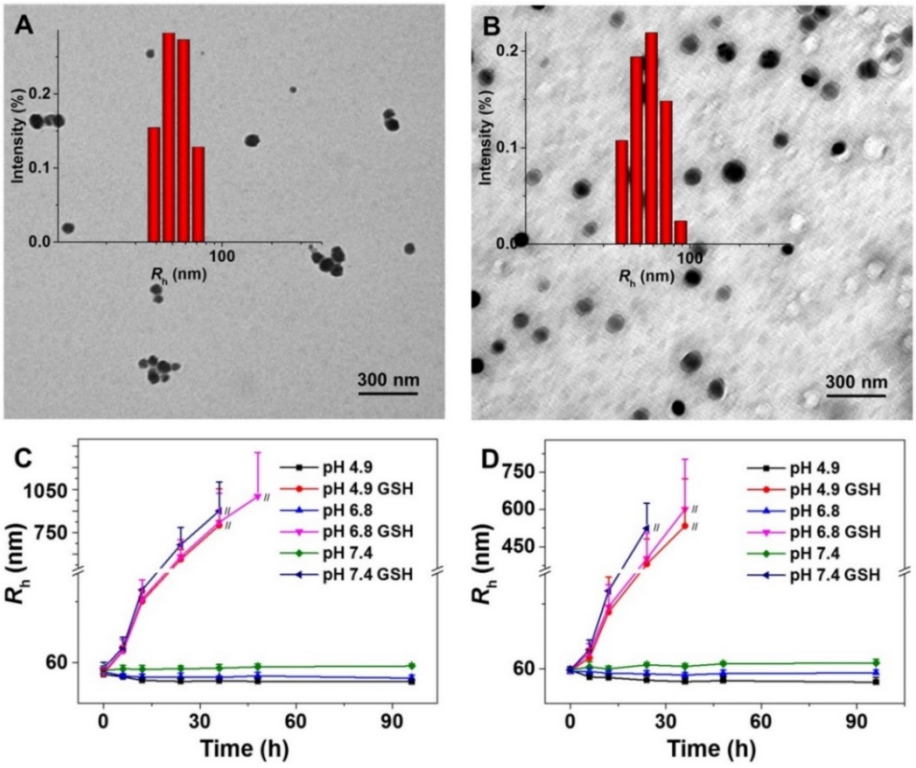

Figure 1. Typical TEM micrographs and R_h of NG (A) and NG/DOX (B). R_h changes of NG (C) and NG/DOX (D) *versus* time in PBS at different pH values (*i.e.*, 4.9, 6.8, and 7.4) without or with 10.0 mM GSH. // represents the interruption of R_h-related light scattering signal.

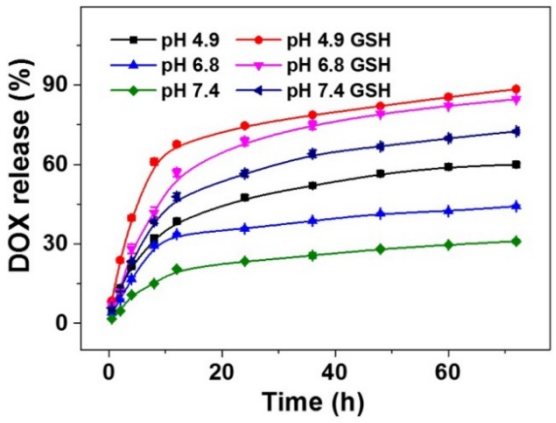

Figure 2. pH and time dual-dependent DOX release from NG/DOX in PBS at pH 4.9, 6.8, or 7.4 without or with 10.0 mM GSH. Each set of data was represented as mean ± SD (n = 3).

To confirm the efficient intracellular DOX release from NG/DOX, CLSM and FCM assays were performed toward HepG2 cells. Cells were pretreated without or with 10.0 mM GSH (GSH− or GSH+) at pH 7.4. For CLSM and FCM detections, cells were then co-cultured with NG/DOX containing 10.0 μg mL^{-1} DOX·HCl equivalent for 2 h; cells without GSH-pretreatment co-incubated with free DOX·HCl was used as a control. As shown in Figure 3A, the red DOX fluorescence was observed to localize in the DAPI-stained nuclei of HepG2 cells for both DOX formulations. The sequence of DOX fluorescence was as follows, from highest to lowest: free DOX·HCl > NG/DOX (GSH+) > NG/DOX (GSH−). It is well known that only the released DOX exhibited observed fluorescence and can be detected by CLSM, and any DOX still incorporated into the core of nanoparticles is not visible due to the self-quenching effect [31]. Therefore, these data clearly demonstrated the efficient endocytosis of NG/DOX and intracellular-responsive DOX release. Moreover, these results paralleled the release behavior observed in PBS under variable conditions (Figure 2). It should be noted that the free DOX·HCl-incubated cells showed the strongest DOX fluorescence in the nuclei. This likely results from the faster diffusion of free DOX·HCl compared with the rate of NG/DOX endocytosis and intracellular DOX release [32]. Additionally, the similar phenomenon was also observed in H22 cells, as shown in supplementary Figure S1.

The efficient cell internalization of NG/DOX was further confirmed by FCM assessment. Mirroring the pattern of DOX release in PBS and CLSM tests, the order of intracellular DOX fluorescence intensity, which should quantitatively reflect the amount of released DOX in the cells, was as follows: free DOX·HCl > NG/DOX (GSH+) > NG/DOX (GSH−) (Figure 3B). This further verified the reduction-responsive DOX release from NG/DOX.

More efficient intracellular drug accumulation should generate a greater ability to inhibit cell proliferation, as has been demonstrated in countless previous work [33]. As expected, the cytotoxicity at 48 h ranked in the order of: free DOX·HCl > NG/DOX (GSH+) > NG/DOX (GSH−) (Figure 4). Furthermore, the half-maximal inhibitory concentrations (IC_{50}s) quantitatively demonstrated the above-mentioned phenomenon. NG/DOX (GSH+) showed a lower IC_{50} (2.3 μg mL^{-1}) than NG/DOX (GSH−) (3.9 μg mL^{-1}), indicating a greater efficacy in the presence of GSH. Of course, free DOX·HCl exhibited the smallest value (1.6 μg mL^{-1}), in agreement with the CLSM and FCM results. For H22 cells, the IC_{50}s of NG/DOX (GSH+) (0.77 μg mL^{-1}), NG/DOX (GSH−) (0.81 μg mL^{-1}), and free DOX·HCl (0.74 μg mL^{-1}) also exhibited the same trend with that of HepG2 cells, as shown in supplementary Figure S2.

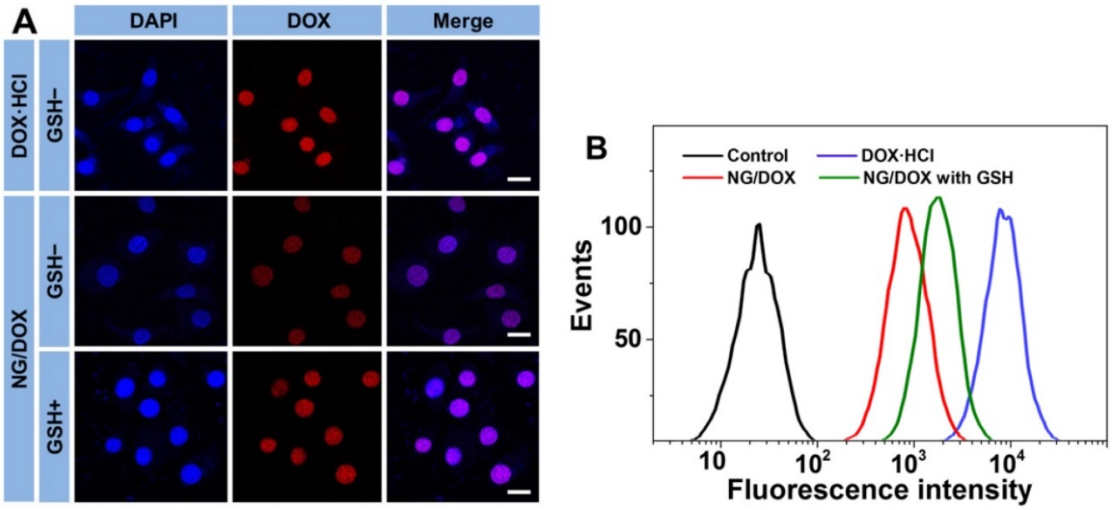

Figure 3. Typical CLSM (A) and FCM determinations (B) of intracellular DOX release from NG/DOX toward HepG2 cells without or with pretreatment of GSH for 2 h (*i.e.*, GSH− or GSH+, respectively). Free DOX·HCl was used as a control. Scale bar = 20.0 μm.

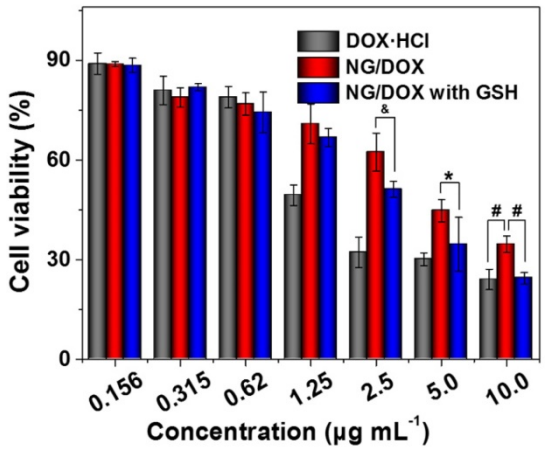

Figure 4. *In vitro* cytotoxicities of NG/DOX against HepG2 cells without or with GSH pretreatment, after incubation for 48 h. Free DOX·HCl was used as a control. Each set of data was represented as mean ± SD (n = 3; * P < 0.05, & P < 0.01, # P < 0.001).

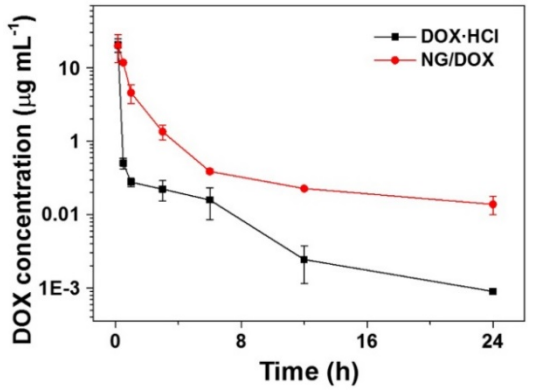

Figure 5. *In vivo* pharmacokinetic profiles after injection of DOX and NG/DOX in rats. Each set of data was represented as mean ± SD (n = 5).

Pharmacokinetics *in vivo*

After intravenous administration, nanoparticles will be diluted with blood and distributed into different compartments of visceral organs (*e.g.*, the liver, spleen, and lung), leaving only small amounts of nanoparticles circulating in the blood. Based on this, to reduce blood clearance and prolong blood circulation time of nanoparticles are key factors for efficient drug delivery to tumor sites [34]. As shown in Figure 5, the plasma pharmacokinetic profiles of free DOX·HCl and NG/DOX were measured by HPLC analyses. The free DOX·HCl disappeared rapidly from the circulation due to its short half-life. In contrast, NG/DOX showed much higher level in the plasma than that of DOX·HCl over the period of test duration. The typical pharmacokinetic parameters were calculated with PKSolver program. The area under the concentration *versus* time curve from 0 to last time t (AUC_{0-t}) of NG/DOX was 25.72 μg (mL h)$^{-1}$, which was 1.4 times higher than that of free DOX·HCl. The peak concentrations (C_{max}s) of free DOX·HCl and NG/DOX were 19.93 and 20.52 μg mL^{-1}, respectively. Their corresponding times to reach peak concentration (T_{max}) were both 0.17 h. The mean half-life time ($T_{1/2}$) of the elimination of NG/DOX was 12.6 h, which was 3.1 times higher than that of free DOX·HCl. Since prolonged blood circulation is the main driving force for passive tumor targeting *via* the EPR effect, NG/DOX has the potential for improved antitumor efficacy *in vivo*.

In vivo antitumor efficacy

Chemotherapy is like a double-edged sword. As mentioned above, high tumor suppression efficacy often coincides with serious side effects. Therefore, the efficacy and safety *in vivo* are the two most important performance parameters for antitumor drug formulations, and both must be thoroughly evaluated before clinical applications of any newly designed formulations. The antitumor capabilities of nanoscale drug delivery systems are generally assessed through tumor growth inhibition assays using tumor-grafted animal models [35, 36]. In this work, the excellent antitumor efficacy of NG/DOX was revealed in an H22 hepatoma-bearing BALB/c mouse model. Treatments included normal saline (NS) and free DOX·HCl or NG/DOX with 3.0 or 6.0 mg DOX equivalent per kg body weight, which were delivered intravenously *via* tail vein injection. Tumor weights were evaluated every two days beginning from the fourth day after inoculation, which was defined as day 1. The first treatment was performed when tumors reached approximately 140 mg, on day 5, after which injections were given once every five days for a total of four injections in 25 days. In addition to monitoring tumor weights over the course of treatment, tumor tissue sections were assessed histopathologically and immunohistochemically at the end of the treatment period. As shown in Figure 6, the tumor indices showed no difference for all the test groups before day 8 (P > 0.05). However, from day 9 forward, variations in the antitumor efficacies of all groups were observed. The tumors of the untreated group grew uncontrollably, and their average tumor index quickly and continuously increased 4.6 times from day 9 to 25, finally reaching ~ 107. Treatment with various DOX formulations suppressed the tumors indices to different extents. Specifically, the tumor indices of the DOX/3.0 group grew slowly; however, the NG/DOX/3.0 group showed lower indices and greater tumor inhibition despite the same DOX·HCl dose of 3.0 mg (kg BW)$^{-1}$ (P < 0.001). Increasing the DOX·HCl dose from 3.0 to 6.0 mg (kg BW)$^{-1}$ improved antitumor efficacy, and both DOX/6.0 and NG/DOX/6.0 showed reduced tumor indices. Again, the nanoparticle formulation NG/DOX/6.0 exhibited an enhanced antitumor

efficacy compared with DOX/6.0. The improved tumor inhibition capacity of NG/DOX *in vivo* at both doses can be attributed to the selective intratumoral accumulation through the EPR effect and the targeted intracellular pH and reduction dual-triggered DOX release.

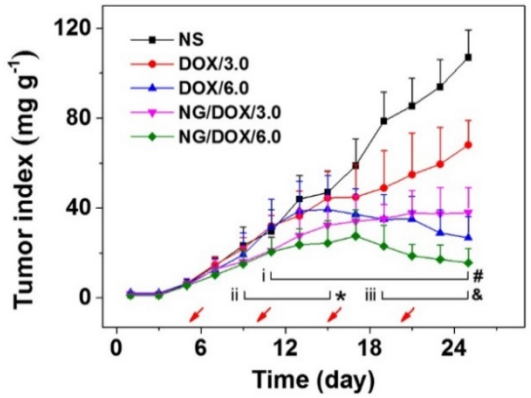

Figure 6. *In vivo* antitumor efficacy of NS, or of free DOX·HCl or NG/DOX at a dosage of 3.0 and 6.0 mg DOX equivalent per kg body weight toward H22-hepatoma-grafted BALB/c mouse model. The treatment times were indicated by the arrows. Each set of data was represented as mean ± SD (n = 10; * P < 0.05, & P < 0.01, # P < 0.001; i, DOX/3.0 *vs* NG/DOX/3.0; ii and iii, DOX/6.0 *vs* NG/DOX/6.0).

Further evidence of the NG/DOX antitumor efficacy was confirmed by both histopathological and immunohistochemical analyses of tumor tissues. On day 25, mice were sacrificed by cervical dislocation, and tumors were isolated for H&E and immunohistochemical staining. H&E staining is the standard for malignancy diagnosis and is indispensable for observing and identifying apoptosis and necrosis of cells or tissue. With H&E staining, nucleic acids are dyed deep blue-purple with hematoxylin, and proteins are nonspecifically stained with eosin. In normal cells or tissue, nuclei are stained blue-purple, whereas the cytoplasm and extracellular matrix have varying degrees of pink staining [33]. As shown in Figure 7, H&E staining of tumor tissue in the control group revealed universal mitosis and minimal signs of hemorrhagic necrosis, which indicated brisk tumor growth. As expected, all the treatments with DOX formulations caused varying levels of tumor suppression. Specifically, they demonstrated decreased mitosis and larger areas of hemorrhage and necrosis. The manifestations of necrosis included nuclear enrichment and/or fragmentation, the dissolution of tumor cells, and the formation of bleeding areas. The relative amount of necrotic tissue for each treatment group ranked as follows: NG/DOX/6.0 > DOX/6.0 > NG/DOX/3.0 > DOX/3.0. Additionally, semi-quantitative data was calculated by Motic Image Advanced 3.2 software (Motic Co., Ltd, Causeway Bay, Hong Kong, P. R. China). As shown in Figure 8A, the NG/DOX group had 1.3 and 1.4 times larger necrotic area than the free DOX·HCl group at the doses of 3.0 and 6.0 mg (kg BW)$^{-1}$, respectively. These results indicated that the degrees of tumor necrosis were consistent with the levels of tumor inhibition.

In recent years, the relationship between macroscopic antitumor efficacies and microscopic immunohistochemical morphologies has attracted more and more attention. In this study, four kinds of immunohistochemical staining – that is, p53, Fas, TNF-α, and cyclin E – were carried out simultaneously to secondarily assess antitumor efficacies of all the test formulations and to explore their antitumor mechanisms from a genetic perspective (Figure 7). Cell apoptosis is mediated by a variety of apoptotic genes. Among them, the caspase family is considered to be the core executor during the apoptosis process. p53 is a tumor suppressor of paramount importance and is the most frequently mutated protein in cancers [37]. Fas is a member of the death receptor family, which is a subfamily of the TNF family. TNF-α is a potent inhibitor of tumor-associated vasculature [38]. Cyclin E, which is highly overexpressed in a variety of cancers, can indicate the growth of cancer [39]. As shown in Figure 7, all the tumor tissue sections in the DOX-formulation-treated groups exhibited greater levels of p53, Fas, and TNF-α compared with the control group, while cyclin E showed the opposite trend. Accordingly, the regulation of all four proteins was amplified as the DOX·HCl dose increased from 3.0 to 6.0 mg (kg BW)$^{-1}$. More interestingly, at both doses, NG/DOX induced greater cell apoptosis compared with free DOX·HCl, as indicated by upregulated p53, Fas, and TNF-α, and by downregulated cyclin E. As with H&E, the semi-quantitative optical densities of all four proteins were calculated by Motic image analysis system. As depicted in Figure 8B, the NG/DOX/3.0 group showed 1.5 and 1.1 times higher p53 signals than the control and DOX/3.0 groups, respectively. NG/DOX/6.0 and DOX/6.0 exhibited both 1.3 times higher signals of p53 compared with NG/DOX/3.0 and DOX/3.0. The Fas signals of NG/DOX/6.0 and NG/DOX/3.0 were 1.2 and 1.2 times higher than those of DOX/6.0 and DOX/3.0, respectively (Figure 8C). The signals from TNF-α followed the same trend of Fas (Figure 8D). Conversely, as shown in Figure 8E, NG/DOX/3.0 and NG/DOX/6.0 displayed a 0.8- and 0.9-fold decrease of cyclin E signals compared with DOX/3.0 and DOX/6.0, respectively. These results showed that NG/DOX can upregulate the expression of pro-apoptotic genes and suppress the expression of anti-apoptotic genes with higher efficiency compared to free DOX·HCl. Hence, the incorporation of

antitumor drug into this smart nanogel has great potential to promote tumor cell apoptosis and inhibit tumor growth in clinical application.

Assessment of safety *in vivo*

At present, almost all formulations of antitumor drugs used in the clinic exhibit some degrees of unfavorable side effects. Moreover, very high tumor suppression efficacy is often accompanied by serious systemic toxicity. For example, platinum-based drug therapy is associated with serious nephrotoxicity and neurotoxicity [24], and various DOX formulations often provoke acute cardiotoxicity and nephrotoxicity [8]. Therefore, the *in vivo* safety of newly designed antitumor drug formulations is another important indicator for future clinical potential. In this work, systematic safety assessments were performed through the surveillance of physical conditions and body weights during the course of treatments, through pathological morphology analyses of various organs after therapeutics, and through examination of BMMR and WBC levels.

The body weights of all H22 hepatoma-grafted BALB/c mice were real-time monitored for 25 days beginning from the fourth day after inoculation. As shown in Figure 9, the body weights of mice from each treated group exhibited a consistent growth trend, and there was no significant difference between any two groups in the initial 1 to 7 days ($P > 0.05$). Later in the treatment stage, *i.e.*, day 9 to 13, the body weights of all DOX-treated mice decreased synchronously with no significant differences among groups ($P > 0.05$). Afterwards, the mouse body weights of NG/DOX/3.0 and NG/DOX/6.0 groups showed a continuous and stable upward trend on day 17 – 25. Within the same time interval, the body weights of mice treated with DOX/3.0 and DOX/6.0 continued on a downward trend and were significantly lower than that of the NG/DOX groups, with the higher DOX·HCl dose resulting in the greatest loss of body weight ($P < 0.001$). The relationship among treatments with various drug formulations and the body weight changes of experimental animals directly indicated drug safety. Treatment with free DOX·HCl at a dose of 6.0 mg (kg BW)$^{-1}$ induced more severe weight loss compared with that at a dose of 3.0 mg (kg BW)$^{-1}$, indicating the dose-dependent side effects of DOX. However, the reversal of body weight loss in mice treated with NG/DOX revealed the improved safety of DOX after being loaded into the pH/reduction-responsive nanogel.

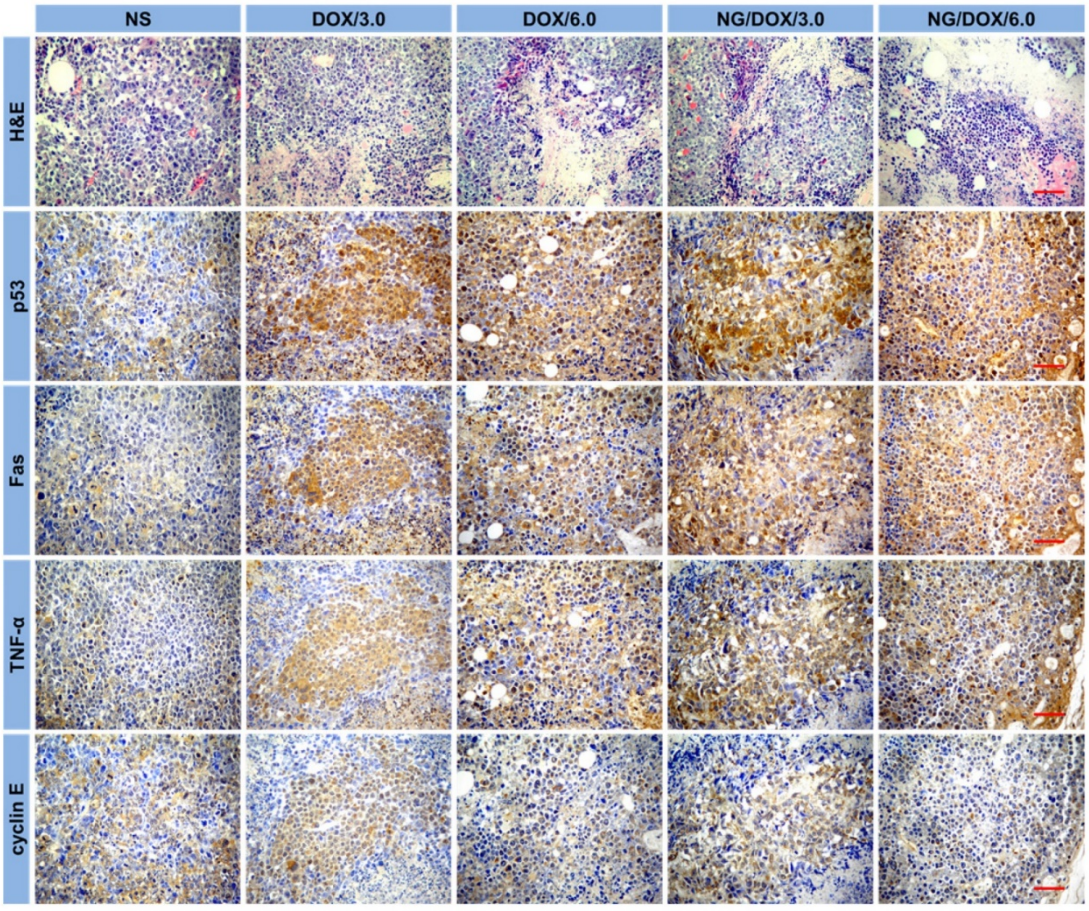

Figure 7. Histopathological (*i.e.*, H&E) and immunohistochemical (*i.e.*, p53, Fas, TNF-α, and cyclin E) analyses of tumor tissue sections after treatment with NS, or with free DOX·HCl or NG/DOX at a dosage of 3.0 or 6.0 mg DOX equivalent per kg body weight. Scale bar = 50 μm.

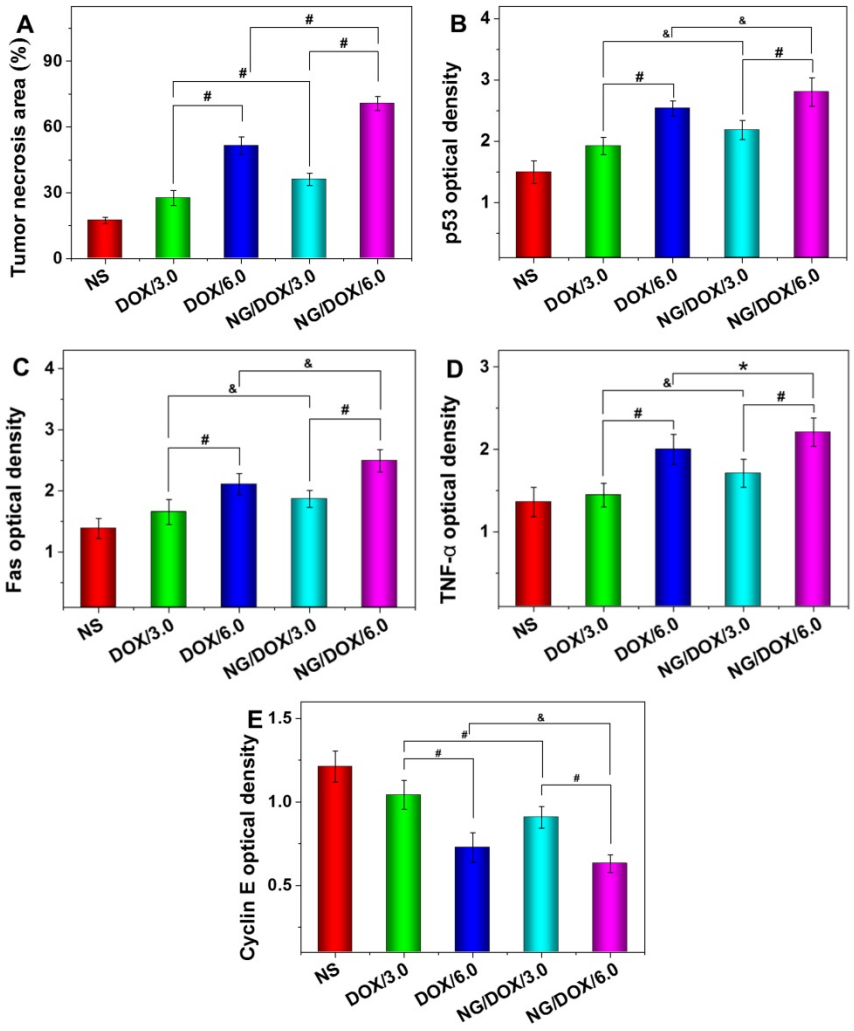

Figure 8. Tumor necrotic area from H&E-stained tumor sections (A), and relative optical densities of tumor sections labeled for P53 (B), Fas (C), TNF-α (D), and cyclin E (E) after treatments with NS, or with free DOX·HCl or NG/DOX at a dosage of 3.0 or 6.0 mg DOX·HCl equivalent per kg body weight. Each set of data was represented as mean ± SD (n = 10; * P < 0.05, & P < 0.01, # P < 0.001).

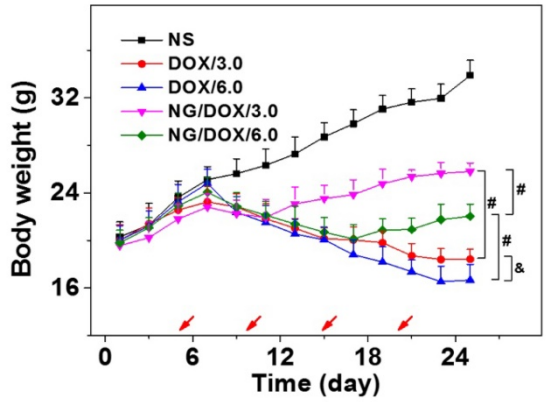

Figure 9. Body weight changes of H22-hepatoma-bearing BALB/c mice in the course of treatment with NS, or with free DOX·HCl or NG/DOX at a dosage of 3.0 or 6.0 mg DOX·HCl equivalent per kg body weight. The treatment dates were indicated by the arrows. Each set of data was represented as mean ± SD (n = 10; * P < 0.05, & P < 0.01, # P < 0.001).

Among other negative physiological effects, chemotherapy drugs can cause genotoxicity. This is commonly quantified by BMMR. The frequency of micronuclei among mouse bone marrow erythrocytes is a direct indicator of chromosomal damage, which can therefore reflect the toxicity of chemotherapy drugs. As shown in Figure 10, bone marrow mononuclear cells were observed in the H&E-stained marrow section from each mouse. The BMMRs were calculated from these histopathological sections (Figure 11A). The BMMRs of H22 hepatoma-grafted mice were significantly elevated with respect to those of normal mice. A dose-correlated increase in BMMR was observed for mice treated with both free DOX·HCl and NG/DOX, but treatment with free DOX·HCl caused significantly greater elevation of BMMR than treatment with NG/DOX (P < 0.001). These results revealed that the physiological damage from DOX administration was dose-dependent, but controlled drug delivery could mitigate the injury

appreciably. To further characterize the impact of DOX chemotherapy on immune status, WBC count was recorded. As depicted in Figure 11B, the WBC count in the NS group was significantly higher than those of the other groups. This indicated that the existence of tumor induced severe inflammation, while treatments with various DOX formulations reduced the inflammation to some extent. These results indirectly indicate the safety of both free DOX·HCl and NG/DOX formulations.

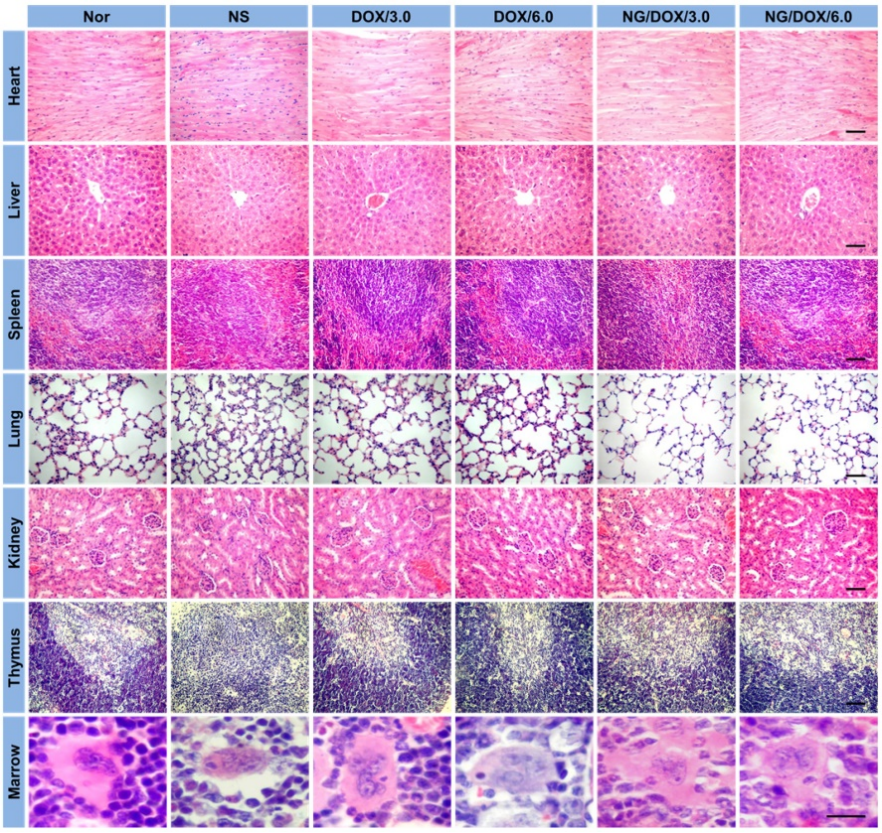

Figure 10. Histopathology analyses of visceral organ sections, *i.e.*, the heart, liver, spleen, lung, kidney, thymus, and marrow, from normal mice (as control, referred as Nor in the figure), or H22-hepatoma-grafted BALB/c mice after treatment with NS, or with free DOX·HCl or NG/DOX at a dosage of 3.0 or 6.0 mg DOX·HCl equivalent per kg body weight. Scale bar = 50 μm.

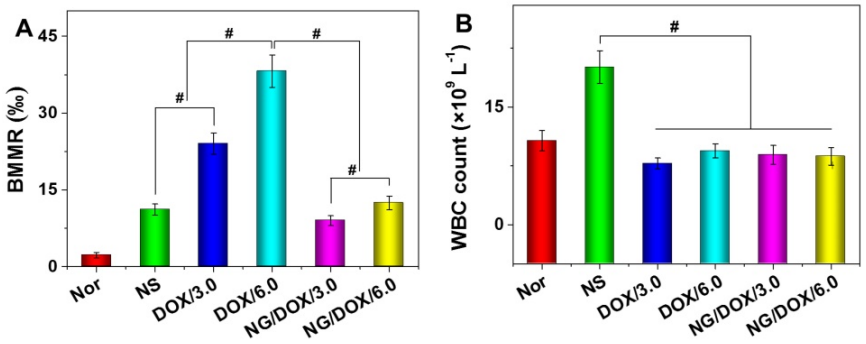

Figure 11. BMMR (A) and WBC count (B) of normal mice (as control), or H22-hepatoma-grafted BALB/c mice after treatment with NS or with free DOX·HCl, or NG/DOX at a dosage of 3.0 or 6.0 mg DOX·HCl equivalent per kg body weight. Each set of data was represented as mean ± SD (n = 10, * P < 0.05, & P < 0.01, # P < 0.001).

Conclusions

In short, a pH and reduction dual-responsive nanogel was prepared with excellent properties, including facile preparation, high drug loading capacity, and ability to favorably respond to different environmental stimuli. Specifically, the nanogel can be efficiently synthesized through the one-step ROP of monofunctional and difunctional amino acid NCAs. The model antitumor drug, *i.e.*, DOX, was loaded into the nanogel with a high DLE of 96.7 wt.%. NG/DOX exhibited an appropriate hydrodynamic radius of about 58.8 nm, which is conducive to selective accumulation in tumor tissue [30]. In

addition, NG/DOX maintained structural integrity and minimal drug release in the circulatory system after intravenous injection. After reaching the tumor tissue through the EPR effect and entering the cells *via* endocytosis, NG/DOX released its payload triggered by the intracellular low pH and high concentration of GSH. Altogether, NG/DOX exhibited excellent tumor inhibition and safety *in vivo*. Of course, other amino-contained hydrophobic and even hydrophilic antitumor drugs and/or contrast agents could also be delivered on-demand efficiently by this smart nanogel with disulfide and carboxyl dual-functionalized core. All of the above advantages confirm the bright prospect of pH and reduction dual-responsive nanogel for upregulate theranostics of malignancy.

Supplementary Material

Supplementary figures.
http://www.thno.org/v07p0703s1.pdf

Acknowledgements

We give our sincere thanks to Elizabeth M Higbee-Dempsey from the School of Medicine at the University of Pennsylvania for reviewing and editing the manuscript. This research was financially supported by the National Natural Science Foundation of China (Nos. 51673190, 51303174, 51603204, 51473165, and 81430087) and the Frontier Discipline Innovation Project of Bethune Medical Department (No. 2013101006).

Competing Interests

The authors have declared that no competing interest exists.

References

1. Choi W, Porten S, Kim S, Willis D, Plimack ER, Hoffman-Censits J, et al. Identification of distinct Basal and luminal subtypes of muscle-invasive bladder cancer with different sensitivities to frontline chemotherapy. Cancer Cell. 2014; 25: 152-65.
2. Narod S. Can advanced-stage ovarian cancer be cured? Nat Rev Clin Oncol. 2016; 13: 255-61.
3. Roth BJ, Krilov L, Adams S, Aghajanian CA, Bach P, Braiteh F, et al. Clinical cancer advances 2012: Annual report on progress against cancer from the American Society of Clinical Oncology. J Clin Oncol. 2013; 31: 131-61.
4. Duncan R. Polymer therapeutics: Top 10 selling pharmaceuticals — What next? J Control Release. 2014; 190: 371-80.
5. Zhang RX, Cai P, Zhang T, Chen K, Li J, Cheng J, et al. Polymer-Lipid Hybrid Nanoparticles Synchronize Pharmacokinetics of Co-encapsulated Doxorubicin-Mitomycin C and Enable Their Spatiotemporal Co-delivery and Local Bioavailability in Breast Tumor. Nanomed: Nanotechnol Biol Med. 2016; 12: 1279-90.
6. Wolfe T, Chatterjee D, Lee J, Grant JD, Bhattarai S, Tailor R, et al. Targeted gold nanoparticles enhance sensitization of prostate tumors to megavoltage radiation therapy *in vivo*. Nanomed: Nanotechnol Biol Med. 2015; 11: 1277-83.
7. Ding J, Shi F, Li D, Chen L, Zhuang X, Chen X. Enhanced endocytosis of acid-sensitive doxorubicin derivatives with intelligent nanogel for improved security and efficacy. Biomater Sci. 2013; 1: 633-46.
8. Xu W, Ding J, Xiao C, Li L, Zhuang X, Chen X. Versatile preparation of intracellular-acidity-sensitive oxime-linked polysaccharide-doxorubicin conjugate for malignancy therapeutic. Biomaterials. 2015; 54: 72-86.
9. Ding J, Xiao C, Zhuang X, He C, Chen X. Direct formation of cationic polypeptide vesicle as potential carrier for drug and gene. Mater Lett. 2012; 73: 17-20.
10. Zhu A, Miao K, Deng Y, Ke H, He H, Yang T, et al. Dually pH/reduction-responsive vesicles for ultrahigh-contrast fluorescence imaging and thermo-chemotherapy-synergized tumor ablation. ACS Nano. 2015; 9: 7874-85.
11. Nukolova NV, Oberoi HS, Zhao Y, Chekhonin VP, Kabanov AV, Bronich TK. LHRH-Targeted Nanogels as a Delivery System for Cisplatin to Ovarian Cancer. Mol Pharm. 2013; 10: 3913-21.
12. Ding J, Xu W, Zhang Y, Sun D, Xiao C, Liu D, et al. Self-reinforced endocytoses of smart polypeptide nanogels for "on-demand" drug delivery. J Control Release. 2013; 172: 444-55.
13. Mura S, Nicolas J, Couvreur P. Stimuli-responsive nanocarriers for drug delivery. Nat Mater. 2013; 12: 991-1003.
14. Tong R, Chiang HH, Kohane DS. Photoswitchable nanoparticles for *in vivo* cancer chemotherapy. P Natl Acad Sci U S A. 2013; 110: 19048-53.
15. Parks SK, Chiche J, Pouysségur J. Disrupting proton dynamics and energy metabolism for cancer therapy. Nat Rev Cancer. 2013; 13: 611-23.
16. Ge Z, Liu S. Functional block copolymer assemblies responsive to tumor and intracellular microenvironments for site-specific drug delivery and enhanced imaging performance. Chem Soc Rev. 2013; 42: 7289-325.
17. McCully M, Hernandez Y, Conde J, Baptista PV, Jesus M, Hursthouse A, et al. Significance of the balance between intracellular glutathione and polyethylene glycol for successful release of small interfering RNA from gold nanoparticles. Nano Res. 2015; 8: 3281-92.
18. Phillips DJ, Patterson JP, O'Reilly RK, Gibson MI. Glutathione-triggered disassembly of isothermally responsive polymer nanoparticles obtained by nanoprecipitation of hydrophilic polymers. Polym Chem. 2014; 5: 126-31.
19. Gauthier MA. Redox-responsive drug delivery. Antioxidants & redox signaling. 2014; 21: 705-6.
20. Maciel D, Figueira P, Xiao S, Hu D, Shi X, Rodrigues J, et al. Redox-responsive alginate nanogels with enhanced anticancer cytotoxicity. Biomacromolecules. 2013; 14: 3140-6.
21. Ding J, Zhuang X, Xiao C, Cheng Y, Zhao L, He C, et al. Preparation of photo-cross-linked pH-responsive polypeptide nanogels as potential carriers for controlled drug delivery. J Mater Chem. 2011; 21: 11383-91.
22. Horigome K, Ueki T, Suzuki D. Direct visualization of swollen microgels by scanning electron microscopy using ionic liquids. Polymer Journal. 2016; 48: 273-9.
23. Xu W, Ding J, Li L, Xiao C, Zhuang X, Chen X. Acid-labile boronate-bridged dextran–bortezomib conjugate with up-regulated hypoxic tumor suppression. Chem Commun. 2015; 51: 6812-5.
24. Li M, Tang Z, Lv S, Song W, Hong H, Jing X, et al. Cisplatin crosslinked pH-sensitive nanoparticles for efficient delivery of doxorubicin. Biomaterials. 2014; 35: 3851-64.
25. Shi F, Ding J, Xiao C, Zhuang X, He C, Chen L, et al. Intracellular microenvironment responsive PEGylated polypeptide nanogels with ionizable cores for efficient doxorubicin loading and triggered release. J Mater Chem. 2012; 22: 14168-79.
26. Ding J, Xiao C, Yan L, Tang Z, Zhuang X, Chen X, et al. pH and dual redox responsive nanogel based on poly(l-glutamic acid) as potential intracellular drug carrier. J Control Release. 2011; 152: E11-E3.
27. Cheng Y, He C, Xiao C, Ding J, Ren K, Yu S, et al. Reduction-responsive cross-linked micelles based on PEGylated polypeptides prepared *via* click chemistry. Polym Chem. 2013; 4: 3851-8.
28. Ding J, Shi F, Xiao C, Lin L, Chen L, He C, et al. One-step preparation of reduction-responsive poly(ethylene glycol)-poly (amino acid)s nanogels as efficient intracellular drug delivery platforms. Polym Chem. 2011; 2: 2857-64.
29. Wilhelm SM, Carter C, Tang L, Wilkie D, McNabola A, Rong H, et al. BAY 43-9006 exhibits broad spectrum oral antitumor activity and targets the RAF/MEK/ERK pathway and receptor tyrosine kinases involved in tumor progression and angiogenesis. Cancer Res. 2004; 64: 7099-109.
30. Li HJ, Du JZ, Du XJ, Xu CF, Sun CY, Wang HX, et al. Stimuli-responsive clustered nanoparticles for improved tumor penetration and therapeutic efficacy. P Natl Acad Sci U S A. 2016; 113: 4164-9.
31. Li D, Sun H, Ding J, Tang Z, Zhang Y, Xu W, et al. Polymeric topology and composition constrained polyether–polyester micelles for directional antitumor drug delivery. Acta Biomater. 2013; 9: 8875-84.
32. Wang J, Shen K, Xu W, Ding J, Wang X, Liu T, et al. Stereocomplex micelle from nonlinear enantiomeric copolymers efficiently transports antineoplastic drug. Nanoscale Res Lett. 2015; 10: 1-11.
33. Huang K, Shi B, Xu W, Ding J, Yang Y, Liu H, et al. Reduction-responsive polypeptide nanogel delivers antitumor drug for improved efficacy and safety. Acta Biomater. 2015; 27: 179-93.
34. Li M, Tang Z, Lv S, Song W, Hong H, Jing X, et al. Cisplatin crosslinked pH-sensitive nanoparticles for efficient delivery. of doxorubicin. Biomaterials. 2014; 35: 3851-64.
35. Adiseshaiah PP, Hall JB, McNeil SE. Nanomaterial standards for efficacy and toxicity assessment. WIRes Nanomed Nanobiotechnol. 2010; 2: 99-112.
36. Ueki N, Wang W, Swenson C, McNaughton C, Sampson NS, Hayman MJ. Synthesis and Preclinical Evaluation of a Highly Improved Anticancer Prodrug Activated by Histone Deacetylases and Cathepsin L. Theranostics. 2016; 6: 808-16.
37. Soragni A, Janzen DM, Johnson LM, Lindgren AG, Nguyen ATQ, Tiourin E, et al. A Designed Inhibitor of p53 Aggregation Rescues p53 Tumor Suppression in Ovarian Carcinomas. Cancer Cell. 2016; 29: 90-103.

38. Uddin MN, Zhang Y, Harton JA, MacNamara KC, Avram D. TNF-α–Dependent Hematopoiesis following Bcl11b Deletion in T Cells Restricts Metastatic Melanoma. J Immunol. 2014; 192: 1946-53.
39. Cheng PH, Rao XM, Duan X, Li XF, Egger ME, McMasters KM, et al. Virotherapy targeting cyclin E overexpression in tumors with adenovirus-enhanced cancer-selective promoter. J Mol Med. 2015; 93: 211-23.